

2012

# Alignment and Composition of Laminin-Polycaprolactone Nanofiber Blends Enhance Peripheral Nerve Regeneration

Rebekah A. Neal

Sunil S. Tholpady

Patricia L. Foley

Nathan Swami

Roy C. Ogle  
Old Dominion University

*See next page for additional authors*

Follow this and additional works at: [https://digitalcommons.odu.edu/medicaldiagnostics\\_fac\\_pubs](https://digitalcommons.odu.edu/medicaldiagnostics_fac_pubs)

 Part of the [Biomedical Devices and Instrumentation Commons](#)

## Repository Citation

Neal, Rebekah A.; Tholpady, Sunil S.; Foley, Patricia L.; Swami, Nathan; Ogle, Roy C.; and Botchwey, Edward A., "Alignment and Composition of Laminin-Polycaprolactone Nanofiber Blends Enhance Peripheral Nerve Regeneration" (2012). *Medical Diagnostics & Translational Sciences Faculty Publications*. 29.

[https://digitalcommons.odu.edu/medicaldiagnostics\\_fac\\_pubs/29](https://digitalcommons.odu.edu/medicaldiagnostics_fac_pubs/29)

## Original Publication Citation

Neal, R. A., Tholpady, S. S., Foley, P. L., Swami, N., Ogle, R. C., & Botchwey, E. A. (2012). Alignment and composition of laminin-polycaprolactone nanofiber blends enhance peripheral nerve regeneration. *Journal of Biomedical Materials Research Part A*, 100A(2), 406-423. doi:10.1002/jbm.a.33204

---

**Authors**

Rebekah A. Neal, Sunil S. Tholpady, Patricia L. Foley, Nathan Swami, Roy C. Ogle, and Edward A. Botchwey

Published in final edited form as:

*J Biomed Mater Res A*. 2012 February ; 100(2): 406–423. doi:10.1002/jbm.a.33204.

## Alignment and composition of laminin–polycaprolactone nanofiber blends enhance peripheral nerve regeneration

Rebekah A. Neal<sup>1</sup>, Sunil S. Tholpady<sup>2</sup>, Patricia L. Foley<sup>3</sup>, Nathan Swami<sup>4</sup>, Roy C. Ogle<sup>5</sup>, and Edward A. Botchwey<sup>1,6</sup>

<sup>1</sup>Department of Biomedical Engineering, University of Virginia, Charlottesville, Virginia 22908

<sup>2</sup>Department of Plastic Surgery, University of Virginia, Charlottesville, Virginia 22908

<sup>3</sup>Office of Animal Welfare, University of Virginia, Charlottesville, Virginia 22908

<sup>4</sup>Department of Electrical and Computer Engineering, University of Virginia, Charlottesville, Virginia 22908

<sup>5</sup>LifeNet Health Institute of Regenerative Medicine, Old Dominion University, Norfolk, Virginia 23529

<sup>6</sup>Department of Orthopaedic Surgery, University of Virginia, Charlottesville, Virginia 22908

### Abstract

Peripheral nerve transection occurs commonly in traumatic injury, causing deficits distal to the injury site. Conduits for repair currently on the market are hollow tubes; however, they often fail due to slow regeneration over long gaps. To facilitate increased regeneration speed and functional recovery, the ideal conduit should provide biochemically relevant signals and physical guidance cues, thus playing an active role in regeneration. To that end, laminin and laminin–polycaprolactone (PCL) blend nanofibers were fabricated to mimic peripheral nerve basement membrane. *In vitro* assays established 10% (wt) laminin content is sufficient to retain neurite-promoting effects of laminin. In addition, modified collector plate design to introduce an insulating gap enabled the fabrication of aligned nanofibers. The effects of laminin content and fiber orientation were evaluated in rat tibial nerve defect model. The lumens of conduits were filled with nanofiber meshes of varying laminin content and alignment to assess changes in motor and sensory recovery. Retrograde nerve conduction speed at 6 weeks was significantly faster in animals receiving aligned nanofiber conduits than in those receiving random nanofiber conduits. Animals receiving nanofiber-filled conduits showed some conduction in both anterograde and retrograde directions, whereas in animals receiving hollow conduits, no impulse conduction was detected. Aligned PCL nanofibers significantly improved motor function; aligned laminin blend nanofibers yielded the best sensory function recovery. In both cases, nanofiber-filled conduits resulted in better functional recovery than hollow conduits. These studies provide a firm foundation for the use of natural–synthetic blend electrospun nanofibers to enhance existing hollow nerve guidance conduits.

## Keywords

biomimetic material; ECM; laminin; nerve regeneration; nanotopography

---

## INTRODUCTION

Peripheral nerve transection occurs commonly in traumatic injury, causing motor and sensory deficits distal to the site of injury. Transection requires appropriate surgical intervention to maximize retention of function and sensation.<sup>1</sup> Reanastomosis by direct suture of the severed nerve fiber endings through the perineurium is the gold standard and results in the best surgical outcome; however, when the nerve retracts after injury and tensionless repair is impossible, cable grafts are often used. Cable grafting takes short nerve segments from a donor nerve and directly reapposes a series of grafts to fill the nerve gap without tension.<sup>2</sup> This procedure leaves deficits at the donor site, and is variably less successful at recovering function at the injury site. To help alleviate donor site morbidity, increased operative time, and size mismatch of the donor nerve, clinicians may choose a nerve conduit for repair of sensory nerves. Conduits currently on the market are biocompatible, biodegradable, hollow tubes into which the nerve ends are sutured. These conduits serve as only an empty, isolated space for growth. Regeneration through nerve conduits typically provides an improvement over no treatment, but for long defects (> 10 mm), conduits often fail due to lack of structural support over the time required for the axon to traverse the gap distance.<sup>3</sup> When axons remain without connection to their target tissue over significant periods of time they lose the ability to regenerate, and the possibility for functional recovery is lost. A decline in the regenerative capacity of both axons and Schwann cells, the support cells of the peripheral nervous system (PNS), begins in humans approximately 8 weeks after injury. At 6 months to 1 year, regeneration is much less likely.<sup>4</sup> This knowledge of the degeneration and regeneration processes has led researchers to the conclusion that, to outperform autografts and allografts, conduits must provide structural support to regenerating axons.<sup>5</sup> To facilitate increased speed of regeneration, in addition to physical support and guidance, the ideal conduit would also provide biochemically relevant signals to guide axonal outgrowth, thus playing an active role in peripheral nerve regeneration.

Multiple strategies exist for improving repair and regeneration with nerve conduits. These involve optimization of cellular components, extracellular matrix proteins, and soluble factors.<sup>6</sup> As occurs *in vivo*, the presence of any one of these three can cause generation of the other two. Extracellular matrix proteins not only present appropriate and recognizable surfaces for interactions such as cell binding and migration, but are able to be manipulated and remodeled by cells to match a more uninjured milieu. Utilizing extracellular matrix components allows for natural cell–matrix interactions to occur such as ligand binding, process guidance, and regeneration, as the substrate can drive cell-fate decisions.<sup>7</sup> These cell-fate decisions *in vivo* are driven by interactions with the dynamic tissue matrix within the extracellular environment.

We have previously shown that electrospun laminin nanofibers can function as a basement membrane mimetic material, both in terms of geometry and composition, driving attachment, differentiation, and process extension of neuron-like or neuronal precursor cells.<sup>8</sup> Electrospinning is an ideal technology to create implantable 3-D scaffold conduits for peripheral nerve regeneration. The resulting isotropic randomly oriented nanofibrous mesh, or anisotropic aligned nanofibrous mesh will provide the necessary structural support and high surface area to volume ratios to facilitate cell migrations required to bridge peripheral nerve gaps to aid in nerve regeneration. Other groups, notably Bellamkonda and coworkers<sup>3,9,10</sup> have filled conduits with thin films of synthetic polymer fibers and found this physical support for outgrowth, along with directional guidance through fiber alignment, support regeneration, and functional recovery across long gaps (>10 mm).

In addition to the physical benefit of providing an aligned substrate for directional outgrowth, there exist two further potential benefits of aligned nanofibers for peripheral nerve regeneration, both occurring as a result of the electric field changes created by the insulating gap. First, high field forces at the edges of the gap exert stronger forces on individual polymer fibers, causing fibers to stretch across the gap, decreasing their resulting diameter. The ideal conditions for alignment and stretching have been explored by our collaborators in a recent publication.<sup>11</sup> This stretching effect decreases the lower bound of mean fiber diameters below 100 nm, yielding fiber diameters mimetic of the natural basement membrane, which has feature sizes in the range of 75–150 nm.<sup>12</sup> Second, fiber alignment across two electrodes separated by an insulating gap results in molecular level orientation of individual polymer molecules within the fiber.<sup>13</sup> Laminin, which contains many biologically active moieties (including IKVAV), may especially benefit from orientation at the individual molecule level in a nanofiber mat. Providing the biologically active molecule laminin within the framework of intraluminal nanofiber scaffold may improve axonal guidance and support during regeneration.

## MATERIALS AND METHODS

### Materials

All cell culture reagents were purchased from Invitrogen (Gibco) unless otherwise noted. Solvents for electrospinning were purchased from Sigma-Aldrich (St. Louis, MO), as was polycaprolactone,  $M_n$  70–90 kDa by gel permeation chromatography (GPC). Laminin was isolated and purified from the Englebreth-Holme-Swarm murine tumor in our laboratory as previously described.<sup>7</sup>

### Cell culture

PC12 cells were obtained from ATCC and maintained in at 5% CO<sub>2</sub> in normal growth medium consisting of Dulbecco's Modified Eagle Medium (DMEM)/F12 (1:1) supplemented with 10% horse serum, 5% fetal bovine serum (FBS), and 1% penicillin–streptomycin. Medium was renewed every 2–3 days as needed, and cells were passaged when cell density approached  $2 \times 10^5$  cells/cm<sup>2</sup>. To assess cell attachment on nanofiber meshes, PC12 cells were plated at an initial seeding density of 10,000 cells/cm<sup>2</sup> in serum-free media conditions. Serum was removed from the media for this assay to ensure

attachment occurred due to the nanofiber geometry or composition, without the serum components that aid in cell–matrix interactions.<sup>14</sup> Substrates were rinsed gently at specific timepoints to remove non-adherent cells. At all time points, cells were provided adequate time for attachment but less time than the reported doubling rate of 48 h.<sup>15</sup> Cells were then fixed for 30 min at room temperature using 4% paraformaldehyde (PFA), stained with 4',6-diamidino-2-phenylindole (DAPI) for visualization, and imaged. For the neurite extension assay with PC12 cells, cells were plated at an initial seeding density of  $2.5 \times 10^4$  cells/cm<sup>2</sup> in serum-free medium onto glass coverslips coated with nanofibers of various compositions. For groups receiving nerve growth factor (NGF) stimulation, NGF was added after 2 h to a concentration of 50 ng/mL. Cells were imaged every day for 5 days in culture. On the 5th day, cells were fixed in 4% PFA for 30 min at room temperature, stained with DAPI for visualization, and imaged. Processes were measured and counted, and statistical comparisons of both length and number were made using a one-way ANOVA with Tukey's *post hoc* testing (Minitab, State College, PA), with significance asserted at  $p < 0.05$ .

Dorsal root ganglia (DRG) were isolated for culture from neonatal FVB/N mice which contain a yellow fluorescent protein (YFP) reporter for  $\beta$ -III-tubulin expression in the developing peripheral and central nervous systems.<sup>16</sup> The DRG were gently plucked from the exposed spinal column, capsules surrounding the DRG were mechanically removed using fine forceps, and the whole DRG body, consisting primarily of peripheral neuron cell bodies, was allowed to attach to the culture surface (tissue culture plastic for control studies, or nanofibers on glass coverslips) in a minimal amount of medium for 2 h before culture medium was added. Growth medium was Ultraculture, with or without 10% FBS, and NGF was added as a growth stimulant up to 100 ng/mL. For neurite extension studies, DRG were allowed to grow in NGF-supplemented medium conditions for up to 5 days. Growth was imaged daily, and on the 4th day, cells were fixed as described above and imaged using both light microscopy and fluorescence to detect the YFP signal. At least three DRG per condition were analyzed, with at least ten processes per DRG measured. Length was measured from the edge of the original DRG body in a straight line to the end of the process farthest from the initial DRG border. Statistical comparisons of length were made using a one-way ANOVA with Tukey's *post hoc* testing (Minitab, State College, PA), with significance asserted at  $p < 0.05$ .

### Blend fabrication

To fabricate blend films or nanofibers, appropriate amounts of dry polycaprolactone (PCL) and laminin were dissolved independently in 1,1,1,3,3,3-hexafluoro-2-propanol (HFP 99.5%, Acros Organics) and then combined to create the desired ratio in solution. For film fabrication, the solution was dispensed onto 12 mm diameter glass coverslips, and the solvent was allowed to evaporate, leaving a thin film of polymer. For electrospun nanofibers, the solution was loaded into a syringe equipped with 18–20 G blunt tipped needle, and mounted into an Aladdin programmable syringe pump (World Precision Instruments, Sarasota, FL). To collect samples for materials analysis such as mechanical testing or scanning electron microscopy (SEM), a collector plate covered with aluminum foil was 10–20 cm below the tip of the needle and electrically grounded. When samples for cell culture were created, 12 mm diameter glass coverslips were placed on top of the grounded

collector plate. A high voltage power supply (Gamma, Ormond Beach, FL) provided positive voltage (10–20 kV), and the syringe pump maintained a steady flow rate (0.5–5 mL/h).

To create patterns for aligned electrospun nanofibers, a conducting material (aluminum or gold) was used to create a gap across an insulating material (glass or air). Aluminum samples were fabricated in the laboratory using aluminum foil and glass coverslips, while gold samples were fabricated by Nathan Swami's group, following previously published protocols.<sup>10</sup> These patterns were utilized in place of the grounded collector described above, and electrospinning proceeded using the same parameters. After electrospinning, all samples, regardless of application, were allowed to dry for at least 24 h and then lyophilized for an additional 24 h to remove any residual solvent.

### Blend characterization

Samples for SEM were cut from the aluminum foil, mounted on aluminum stubs (Electron Microscopy Sciences, Hatfield, PA), sputter coated with gold using a BAL-TEC SCD005 sputter coater, and imaged using a JEOL JSM6400 SEM with Orion image processing at 15 kV accelerating voltage. Diameter measurements were made using the measure tool in Image J (open source software available through NIH), with at least 50 measurements per sample of a minimum of three images from different electrospun samples. Care was taken that each measurement represented an independent fiber in the image.

Fourier transform infrared (FTIR) spectroscopy was used to characterize the blend mesh components, to ensure both PCL and laminin spectra were visible. An Alpha FTIR spectrometer (Bruker Optics, Inc., Billerica, MA) was used in attenuated total reflectance mode. Dry polymer samples, stock polymer as received or isolated, or polymeric nanofiber meshes were placed on the field and analyzed. Spectra were generated using Opus software and compared for characteristic peaks of both PCL and laminin.

For mechanical testing, rectangular samples at least 10 mm in length and 5 mm in width were separated from the aluminum foil and mounted onto mechanical grips on an Instron 5543 (Instron, Norwood, MA) using BlueHill 2 software. An initial strain of 0.2% was set, and the sample was loaded uniaxially at a rate of 10% strain per minute. Stress versus strain curves were measured and characterized by Young's modulus, yield strength, and ultimate tensile strength (UTS). A minimum of three rectangular samples per group were tested.

For GPC to determine molecular weight changes and degradation properties over time in aqueous media, nanofiber meshes were incubated in PBS at 37°C with gentle agitation for up to 6 weeks. At each time point, PBS was aspirated and samples were lyophilized overnight to remove residual solvent. Samples were then dissolved in HPLC-grade tetrahydrofuran (THF), filtered through 0.2 µm filter, and loaded into vials with a septum for GPC. Molecular weight was measured by GPC (THF, 20°C, 1.0 mL/min) against polystyrene standards on a Hewlett-Packard instrument (series 1100 HPLC) equipped with Polymer Laboratories 5 µm mixed-C columns and connected to refractive index (Viscotek LR 40) detector. Data were processed with the OmniSEC software (version 4.2, Viscotek Corp).

Alignment was characterized utilizing both manual angular orientation measurement as well as calculating the vector produced by Fast Fourier Transform (FFT) of the image. For angular measurements, the axis of alignment was chosen as perpendicular to the conducting electrode edge, and fiber angles were measured from that axis. A minimum of 20 angular measurements were made per image with a minimum of three images used, each of different electrospun samples. Applying FFT methods to digital images yielded a frequency domain representation. In addition, a magnitude plot of the frequency domain provided information about the orientation of edges present in the image. Scanning electron micrographs were submitted to FFT. When the edges of the fibers were parallel to each other, as in the aligned samples, the FFT displayed a narrow distribution of intensities around a center which indicated the direction perpendicular to the edge orientation. When edges of the fibers were random, the intensity distribution widened into a circular distribution. To quantify the intensity distribution, the mean intensity was computed at various angles about the center of the image in a circular ring with inner radius equal to one eighth and the outer radius equal to one quarter of the image size. From this mean intensity plot, full width at half maximum about the peak intensity value were calculated. When normalized with respect to 180°, this distribution yielded a value between zero and one, defining the degree of alignment of the edges in that image. In this distribution, zero represented completely random, or lack of, orientation, and one represented completely aligned nanofibers.

#### **Rat tibial nerve transection and conduit repair**

To create PCL microfiber conduits for the *in vivo* study of laminin–PCL blend nanofiber meshes, 1.6 mm diameter stainless steel rod (McMaster-Carr, Los Angeles, CA) was cut to 30 cm length and mounted into a custom, self-centering chuck connected to a motor (ZDM3581T, Baldor Vector Three Phase Motor and H2 Vector Drive, Ft. Smith, AK) using non-conductive couplers. The chucks slid on a custom rail with a freely rotating tail chuck, and the entire system was housed in a 1/2 inch thickness high-density polyethylene (HDPE) enclosure. An initial solution of 20% (w/v) PCL in HFP was loaded into a syringe, mounted in the syringe pump (Aladdin 1000, World Precision Instruments, Sarasota FL), and situated 12–14 cm away from the center of the rotating mandrel. The positive voltage lead of the high voltage source (Gamma, Ormond Beach, FL) was connected to the 18-G needle, and the mandrel was grounded using the ground lead. Mandrel rotation speed was set to 100 rpm to prevent mechanical alignment that occurs with higher rotation speeds. The solution was dispensed at 2 mL/h, and simple translating motion was used to ensure complete coverage of the 30 cm mandrel. After electrospinning, the conduit material was dried under vacuum, then cut into 15 mm segments and removed from the stainless steel rod and sterilized for implantation. The resulting conduit had an inner diameter of 1.6 mm and a length of 15 mm. Nanofiber sheets of randomly oriented PCL nanofibers, randomly oriented 10% laminin nanofibers, or longitudinally aligned PCL nanofibers were folded in half and placed into the lumen of the conduit. Conduits were sterilized under ultraviolet (UV) light overnight, followed by two 30 min washes in 70% ethanol and three 30 min washes in sterile water. Conduits were maintained in sterile phosphate buffer solution (PBS) until implantation.

Female Sprague Dawley rats weighing 250 g at the time of surgery were anesthetized using isoflurane to effect and maintained under anesthetic for the duration of the procedure. The

surgical site was shaved and prepped using aseptic technique, and ketoprofen (4 mg/kg) was administered subcutaneously as an analgesic to relieve post-operative pain. A skin incision was made along the length of the tibial axis on the medial side of the lower extremity, providing access to the tibial nerve. The nerve was gently freed from the surrounding musculature and transected. A 5-mm segment was removed and the nerve was allowed to retract, leaving a 10-mm gap between the proximal and distal ends. The 15-mm conduits were placed in the gap, and nerve stumps were pulled 2.5 mm into each end and sutured through the epineurium with 10-0 nylon suture (Ethilon). The incision was closed using subcuticular 4-0 vicryl sutures (Ethilon) and sealed with VetClose (Butler Animal Health Supply, Dublin, OH). Bitter orange ointment (ARC Laboratories, Atlanta, GA) was applied to the foot to prevent self-mutilation. Ketoprofen (4 mg/kg) was administered subcutaneously once daily as an analgesic for 3 days post-surgery, and rats were housed separately with access to food and water *ad libitum* in a 12 h light/dark cycle for the duration of the study. Weekly motor and sensory follow-up testing was conducted on all experimental groups.

### Motor and sensory testing

To examine sensory recovery, measurement of thermal withdrawal latency was conducted using a paw thermal stimulator which measures the latency interval between stimulus application and paw lifting. This method has been previously described for analysis of sensory function in lower limb nerve injury.<sup>17</sup> Briefly, the plantar test system consisted (IITC Life Science, Woodland Hills, CA) consisted of a plastic chamber that sat on a clear elevated floor and was temperature regulated at 30°C. Animals were allowed to acclimate in the chamber for 15 min. A radiant heat source mounted on a movable holder beneath the glass floor was used to deliver a thermal stimulus to the plantar side of the hind paw. To prevent thermal injury, the light beam was programmed to stop automatically after 20 s if the animal failed to withdraw its paw. Baseline levels were determined prior to surgery, and the thermal intensity was adjusted to provide a 4–6 s latency period in normal, non-injured rats. At least three latencies were measured for each hind paw per test session. The three scores were averaged and compared using a general linear model ANOVA with crossed factors and Tukey's *post hoc* testing with significance asserted at  $p < 0.05$ .

To assess motor recovery, walking track analysis was performed to assess the animals' mobility and gait. The hind feet were dipped in dilute India ink, and the rats were allowed to walk down a 10 cm × 60 cm corridor into a darkened box. The floor of the corridor was covered with removable paper used to record the animals' paw prints. At least three clear paw prints were selected from each walking track and the parameters of print-length, toe-spread (distance between first and fifth toes), and intermediary toe-spread (distance between second and fourth toes) were measured, as these particular measurements have been shown to be most indicative of specific gait changes due to tibial nerve injury. The contralateral paw print was measured to determine the normal values and calculate the print length, toe spread, and intermediary toe spread factors. In all cases the maximal distance was measured. The formula of Bain et al. was used to calculate the tibial function index (TFI) with a value of 0 representing normal function and a value of –100 indicating complete loss of function.<sup>18</sup> Both the TFI and the toe spread factor for animals from each group were

compared using General Linear Model ANOVA with crossed factors in Minitab 15 statistical software. Pairwise comparisons were made with Tukey *post hoc* test, with significance asserted at  $p < 0.05$ .

### End-point testing: Electrophysiology and histological analysis

At the end of the study, animals were tested for nerve conduction and electromyography (EMG) before tissue was harvested for histology, following established protocols.<sup>8</sup> For electrophysiology, the animal was anesthetized and the initial surgery site exposed. The conduit or healthy tibial nerve and a small segment proximal and distal to the injury were freed from surrounding tissue. Neurosign disposable bipolar probes (Magstim, Wales, UK) were placed on the exposed sections, 15 mm apart. Both proximal and distal electrodes were stimulated in turn, utilizing a square pulse of 0.02 ms duration and 10–20 V amplitude on a Teca Synergy N-EP system (Oxford Instruments, Oxfordshire, UK). To ensure the conduits themselves were not providing a means for electrical conduction, both electrodes were placed on the surface of the conduit and were stimulated in each direction. For assessment of muscle reinnervation, the distal electrode was moved to the surface of the gastrocnemius muscle to record EMG activity.

After electrophysiology, animals were euthanized and tissue was harvested and fixed overnight in 4% paraformaldehyde. Post-fixation, samples were moved to 30% sucrose in PBS solution for up to 3 days at 4°C, after which samples were imbedded in O.C.T. Compound (Tissue Tek) and frozen for cryostat sectioning. Using a Leica CM1950 Cryostat (Leica, Wetzlar, Germany) 8–14 micron thick sections were cut from either transverse or longitudinal sections of the nerve, and immunohistochemistry or hemotoxylin and eosin (H&E) staining were performed to indicate tissue morphology and the presence of regenerating axons (NF160, 1:500, Abcam). For immunohistochemistry, sections were washed in 0.1% saponin in PBS and incubated in a blocking solution consisting of 4% normal goat serum (NGS), 1% bovine serum albumin (BSA), and 0.1% saponin for 1 h at room temperature. Primary antibody was reconstituted in the blocking solution and applied to sections. Sections were then incubated overnight at 4°C. Before application of the secondary antibody, samples were washed in 0.1% saponin in PBS. Sections were then incubated in dilutions of secondary antibody (Alexa Fluor546 goat anti-rabbit IgG) for 1 h at room temperature. Sections were washed, dried, and mounted using VectaShield hard mount with DAPI (Vector Laboratories, Servion, Switzerland). Sections were imaged using a Nikon Eclipse C1 confocal microscope.

## RESULTS

### Blend fabrication and characterization

To characterize the blended laminin–PCL nanofibers, we examined mesh morphology using SEM, polymer content using FTIR, changes in mechanical properties using uniaxial tensile testing, and degradation properties using GPC. We successfully fabricated blend nanofiber meshes containing 1% and 10% laminin content by weight, as shown in Figure 1(A,B). The fiber diameters of these meshes were measured from 100 to 200 nm in mean diameter, within published ranges of native basement membrane feature size [Fig. 1(C)].<sup>11</sup> As

previously described,<sup>7</sup> minimal beading in the mesh is reminiscent of the structure of basement membrane, so when optimizing nanofiber formation, minimal beaded structures were allowed to remain.

To ensure both PCL and laminin were present in the blend meshes, we considered the FTIR spectra [Fig. 1(D)]. The FTIR spectra describe the bond angles present in the sample, and when used in attenuated total reflectance (ATR) mode, nanofibers can be used as the sample for analysis. Characteristic peaks of each polymer are indicated on the spectra and confirmed the presence of both polymers. Interestingly, increasing laminin content yielded greater laminin peaks and higher PCL content yielded greater PCL peaks in near proportion to respective compositions. Since samples of similar total polymer content were used for analysis, it is possible that signal strength in this case does correlate with amount of polymer present.

Uniaxial tensile testing satisfied our concern that laminin content may affect critical mechanical properties of the mesh. Since significant tension should not be experienced in the healing environment of the peripheral nerve, and in fact surgeons strive to create a tensionless environment using nerve guidance conduits, minor differences in tensile strength should not lead to conduit failure. When comparing Young's modulus, UTS, and yield strength, a range of comparisons which span the stress-strain curve of these materials, we saw no significant difference among the blends of various laminin content [Fig. 2(A-C)]. In addition, to show that laminin content at or below 10% of the total polymer weight did not play a significant role in the degradation properties of the material, we compared weight-averaged molecular weight ( $M_w$ ) by GPC over 6 weeks, the length of our preliminary *in vivo* study. From this analysis, shown in Figure 2(D), we observed no significant difference in  $M_w$  over time. For the considerations of nerve repair, we found no detriment in terms of mechanical or degradation properties to prohibit the use of laminin as up to 10% polymer weight as a substrate for regeneration.

### Assessment of bioactivity

Having chosen laminin specifically for its inherent properties which promote cell attachment and neurite extension, we sought to verify that this material does indeed retain these properties after processing into a blended nanofiber with the synthetic polymer PCL. In order to understand the amount of laminin required per amount of PCL using the traditional two-dimensional culture method, and to provide a starting point for fabrication of blend nanofibers, studies were first performed using laminin and laminin-PCL blend films. These studies showed 10% laminin content in film substrates for cell culture yielded process extension from murine DRG of length and number not statistically different from that on 100% laminin (Fig. 3). While further studies may elucidate the threshold content for laminin activity, for the remainder of our studies, we established 10% laminin content as sufficient to maintain bioactivity.

Moving forward from two-dimensional films to nanofiber studies, PC12 cells were chosen for their neuron-like process extension, but provide an additional benefit here: they will not remain attached to tissue culture polystyrene without serum unless an adhesive surface is provided. To ascertain that laminin maintains its cell adhesive properties when blended with

PCL, PC12 cell attachment was investigated [Fig. 4(A)]. After 24 h, sufficient time for attachment but less than the doubling time of the cells, attachment to blend meshes was quantified. While very few cells were able to attach to PCL nanofibers alone, no significant difference in attachment was observed between 10% and 100% laminin nanofibers. In addition, to consider the feature of PC12 cells more relevant to clinical application in peripheral nerve regeneration, we examined PC12 process extension on blend nanofibers. We found PC12 cells extend processes longer than the diameter of the cell body on blend nanofiber substrates, regardless of whether NGF is provided as a soluble signal.

To further verify that blending laminin with PCL during nanofiber fabrication allows for the retention of laminin bio-activity, we assessed neurite outgrowth from murine DRG over a 4-day period on 100% and 10% laminin nanofibers. Utilizing a  $\beta$ -III-tubulin driven YFP reporter transgenic mouse, we were able to record the functional outcome of  $\beta$ -III-tubulin expression in our studies as well. In Figure 4(B–D), we saw significant outgrowth all around the DRG, regardless of whether laminin content of the nanofibers was 10% or 100%, and were able to detect no difference in length of processes. In addition, primary neurons dissociated from DRG were observed to extend processes on blend nanofibers with no significant difference in length or number of processes than seen in previous studies on pure laminin nanofibers.<sup>7</sup> We chose neurite length as the metric for comparison because length, rather than number, size, or another metric, is most indicative of the time to healing of an injured nerve fiber. Longer extensions equate to faster regeneration, and atrophy of the end organ is prevented when a functional connection is made, even if that connection is weaker (fewer axons) than the original connection. Once the functional connection is successful, the nerve can continue to grow and expand its number of axons and the number of myelinated axons.

### Oriented nanofiber meshes and directional outgrowth

Though laminin nanofibers, or PCL–laminin blend nanofibers with at most 10% laminin content, provide sufficient cues to encourage attachment and outgrowth, we fabricated aligned nanofiber meshes to further improve outgrowth speed and direction for application to peripheral nerve regeneration. Utilizing the insulating gap method discussed by our colleagues<sup>10</sup> and others,<sup>19</sup> we successfully fabricated aligned nanofibers containing 10% laminin [Fig. 5(A)]. A secondary benefit of alignment using this method is the stretching of nanofibers across the gap and resulting decrease in fiber diameter. In this case, we see significant stretching of fibers across the gap regardless of the initial total polymer concentration (5% or 8% w/v, both with laminin comprising 10% of the total polymer mass), pulling our average fiber diameter down to approximately 100 nm [Fig. 5(B)]. In addition, we have characterized the alignment of these meshes using both manual calculations [Fig. 5(C)] and FFT [Fig. 5(D–F)]. Both indicate significantly greater alignment than nanofibers electrospun onto a grounded plate collector lacking the insulating gap, and minimal differences between laminin–PCL and PCL groups.

### Rat tibial nerve transection recovery

To examine our blend and aligned meshes in the *in vivo* regenerative environment, we inserted the nanofiber meshes into PCL microfiber conduits (Fig. 6), implanted them into the

severed tibial nerve, and examined motor and sensory recovery over a 6 week time course. To assess the effects of both composition and geometry on recovery, we inserted meshes of PCL and laminin–PCL blend in random and longitudinal orientation. Because the tibial branch of the sciatic nerve is a mixed nerve, containing both motor and sensory fibers, we followed the animals' progress in recovery of both functions, as functional recovery is the critical outcome in patient care. Sham and empty conduit surgeries verified (1) the surgery itself does not result in functional deficit without severing the nerve and (2) we successfully created a defect which would not heal during the course of our study.

In our observations of thermal withdrawal latency (sensory function), no statistical differences were observed among the weeks of the sham surgery group [Fig. 7(A)]. When comparing across experimental groups, PCL random, PCL aligned, and laminin–PCL random groups were significantly different from both the sham group and the laminin–PCL aligned group ( $p < 0.01$ ), and all groups were significantly different from the hollow group ( $p < 0.01$ ). In addition, PCL nanofibers, either random or aligned in configuration, had significantly lower latencies and faster recovery than the laminin–PCL random group ( $p < 0.01$ ). In considering the differences among the weeks of surgery, the most dramatic healing occurs between weeks 4 and 5. Week 4 is significantly different from week 6 ( $p < 0.01$ ); however, latencies at weeks 5 and 6 are not significantly different ( $p = 0.322$ ). Individual group and week comparisons are indicated in Figure 7(A). Observing the overall trends, we found laminin–PCL aligned nanofibers to show latencies similar to sham surgeries across the timepoints, while nanofibers of the same composition but without alignment (laminin–PCL random) were more similar to hollow conduits. However, regardless of composition and orientation, all animals with nanofibers inside the conduit showed some recovery of function over the 6-week time period.

While improved sensory function is ideal, recovery of motor function is also of importance in the clinical setting, as complete mobility is desirable. With the tibial nerve transection injury, all animals were able to adapt and continue using both hind legs to ambulate. In addition, little self-mutilation of the injured foot was observed, suggesting this model is well-suited to study as the animals maintain relatively normal daily functioning capacity, but still show changes in gait analysis with injury which can be measured and applied to a modified tibial function index.<sup>17</sup> Animals with tibial nerve transections show shortening of both toe spread and intermediary toe spread, but little change in print length. For that reason, we compared toe spread, the distance between the first and fifth toes, across all groups and time-points. All animals that received conduits with nanofibers show some return of function, while those with empty conduits show small changes in toe spread which may be a result of adaptation to the injured state, but no steady return to standard print features [Fig. 7(B)]. A statistically significant difference was found between the group receiving PCL random nanofibers and the hollow control ( $p = 0.013$ ) or the 10% laminin blend random nanofibers ( $p = 0.011$ ). Laminin blend aligned nanofibers showed better healing when compared to hollow conduits ( $p = 0.062$ ) and to laminin blend random nanofibers ( $p = 0.66$ ); however, neither composition of randomly oriented fibers were significantly different from animals receiving hollow conduits. Individual groups and weeks were compared using Tukey's *post hoc* testing, but no significant differences were found, most likely due to the high variation in measurements.

At the end of the 6-week study, the surgical site was reopened for nerve conduction and EMG assessment. Nerve conduction speeds across the healthy control tibial nerve in each animal were consistent with literature reported values.<sup>20</sup> In addition, no measurable conduction was observed across the exterior of the conduits, or across unused conduits. This finding is as expected, as most groups add dopants to PCL when electrical conductivity is desired.<sup>21,22</sup> Animals with no nanofibers within the lumen of the conduit showed no nerve conduction or muscle activity when the proximal or distal end of the severed nerve was stimulated; however, animals which received nanofibers within their conduits, regardless of the composition or orientation, showed some recovery of nerve-to-nerve and nerve-to-muscle conduction [Fig. 8(A–C)]. When only retrograde conduction was considered, a significant difference was evident in conduits containing aligned nanofibers of either composition over those containing randomly oriented PCL or laminin-PCL blend nanofibers [Fig. 8(D)]. Although nerve conduction velocity does not provide a complete picture of regeneration within the nerve, this standard metric serves as an indicator of axonal regeneration and re-myelination.<sup>8</sup>

These results were supported by H&E sections and immunohistochemistry for regenerating axons (NF160). Representative images in Figure 9 indicated some axonal outgrowth, represented by positive staining for NF160, an axonal marker, into conduits containing either composition of random nanofibers, though this outgrowth fails to show an appropriate linear organization from proximal to distal stump. In conduits which contained either composition of aligned nanofibers, greater tissue coverage and axonal outgrowth, indicated by positive NF160 staining, is apparent, and the tissue shows a level of organization in the longitudinal direction that does not exist in the other groups. The greatest axonal coverage occurred in the group receiving aligned laminin–PCL blend nanofibers, supporting the findings of the nerve conduction study and motor and sensory tests. These findings were supported by H&E transverse cross-sections (Fig. 10), which show increasing tissue formation and infiltration into the conduit for groups with aligned fibers, and specifically for the group containing laminin–blend aligned nanofibers.

## DISCUSSION

Nerve transections are the model of choice among researchers studying peripheral nerve injury for two reasons: (1) lacerations resulting in nerve transections make up 30% of serious nerve injuries and (2) injury and healing in this model are well characterized in both the research and clinical setting. In the distal portion of the injured nerve, Wallerian degeneration proceeds rapidly: axons and myelin fragment within hours of injury, and neurofilaments and tubes lose their ordered structure. With disruption of axonal continuity, all electrical conduction across the injury site is lost. Schwann cells achieve an activated state and function to aid macrophages in the removal and clearance of the injury site. In the proximal segment, degeneration proceeds similarly, but may be local (only affecting a small portion of the proximal segment) or may degenerate all the way to the axonal cell bodies. In transection injuries, regeneration only begins after Wallerian degeneration is complete, increasing the time to reinnervation and decreasing the probability of functional recovery.<sup>1</sup> For this reason, focus has been placed on increasing the speed and efficiency of axonal

regeneration through biochemical and physical surface cues to aid healing and potentially recover function over larger gaps than previously thought possible.

### Blend fabrication and characterization

Previously, we showed successful fabrication of laminin nanofibers and their utility for *in vitro* attachment and neurite extension. To improve processing capabilities, a synthetic, biodegradable polymer PCL was blended with laminin and blend nanofibers of similar dimensions were fabricated. FTIR spectroscopy confirmed the presence of both polymers in blend nanofibers, and analysis of the relative proportions, demonstrating production of blend nanofibers with specific laminin content. When compared with literature spectra for both PCL<sup>23</sup> and laminin,<sup>24</sup> characteristic peaks of both polymers were evident, validating the blend fabrication methodology. This method of blending synthetic and natural polymers has been used with varying degrees of success by other groups using different polymer combinations,<sup>25</sup> but we are the first to specifically electrospin blended PCL and laminin nanofibers for the purpose of enhancing axonal outgrowth in peripheral nerve repair.

Before examining the bioactivity of our laminin nanofibers, blend meshes were characterized to ensure other differences in the mesh characteristics such as mesh morphology, mechanical properties, and degradation rates would likely not affect cell behavior. The blend nanofibers have mean fiber diameters ranging from 100 to 200 nm which is within the reported range of basement membrane.<sup>11</sup> These dimensions suggest that like pure laminin nanofibers, they can mimic the fiber geometry of the basement membrane. Tensile properties of the mesh were also equivalent regardless of laminin content of the mesh, mostly likely because the tensile strength of PCL is great enough to withstand such minimal additions of laminin. Uniaxial tensile properties are important; a source of failure is due to tensile forces caused by patient movement beyond the bounds of the elastic region of the conduit. With all inner conduit materials maintaining no detectable differences in elastic modulus, yield strength, or UTS, we can be confident that minimal mechanical differences will not likely affect measured outcomes. In addition, the values we calculated for tensile properties are in agreement with the literature regarding PCL nanofibers.<sup>26</sup> Finally, the degradation rates found by GPC are consistent with published PCL degradation rates,<sup>27</sup> and show no significant differences among groups over time. These data verify that while laminin may prove a useful additive to these meshes, it does not affect the bulk degradation properties. Since all measured mesh characteristics remain consistent regardless of the laminin content, it's likely differences in cell behavior on the mesh are due specifically to the laminin content and mesh orientation. As with all characterization metrics, mechanical properties and degradation rate may vary *in vivo* from assessments made *in vitro*, as the more complex environment, immunological response, and movement of the animal may all affect the properties of the conduit long-term. Nonetheless, these benchtop characterization methods provide insights into how the conduit and scaffold materials may function *in vivo*, and help elucidate the important features of the conduit.

### Assessment of bioactivity

For the purposes of these studies, laminin bioactivity is defined as the ability to promote cell attachment and neurite outgrowth. The bioactivity of various blends of laminin with PCL, in

comparison to laminin nanofibers alone, was assayed with both PC12 cells and murine DRG. While it has typically been reported that substrate with nanotopography such as our nanofiber meshes will encourage greater cell attachment due to greater surface area, the presence of laminin was evaluated for deleterious or synergistic effects on cell attachment. We previously reported that pure laminin nanofibers promote significantly greater and faster cell adhesion than laminin films,<sup>7</sup> suggesting the relevance of the nanofiber geometry for attachment; however, in comparison with pure PCL nanofibers, even 10% laminin content provides for significantly greater cell attachment. Laminin therefore may be critical in encouraging faster regeneration in a multitude of settings, since cell adhesion is often a bottleneck step which impedes synthetic polymer success for tissue engineered scaffolds. In addition, Pierucci et al. cultured primary Schwann cells on PCL membranes, and found they do not attach as well as to poly(lactic acid) (PLLA) membranes.<sup>28</sup> As Schwann cells actively secrete basal lamina and neurotrophic factors to modify the peripheral nerve microenvironment, especially after injury and during regeneration, Schwann cell attachment is crucial to successful regeneration. The addition of laminin to PCL nanofibers should improve Schwann cell attachment, which in turn increases basal lamina secretion and the production of neurotrophic factors which support and guide the regenerating axon. While these studies examined PC12 cell attachment as a representative measurement of how cells will likely behave on the mesh, future studies will explore how primary Schwann cells respond to the composition and alignment of the mesh.

While successful cell adhesion to our scaffold is crucial, we hope to utilize the intrinsic neurite promoting properties of laminin to encourage outgrowth beyond what is obtainable with synthetic polymers. Several groups have reported the necessity for axonal adhesion to the growth surface in order to produce the engorgement of growth cones and subsequent formation of a new axonal length.<sup>29,30</sup> Observed PC12 cell and murine DRG attachment and neurite extension support this conclusion regarding laminin blend nanofiber substrates. We observed greater neurite length from DRG on laminin substrates, as well as a greater percentage of PC12 cells extending processes with or without NGF stimulation. These data lead us to conclude that while there may be cases where adhesion to a substrate is detrimental, in the case of laminin, which contains specific axonal outgrowth and growth cone guidance domains, cell or neurite attachment does not prohibit outgrowth. In fact, we find laminin content at or above 10% total polymer weight enhances the capacity for process outgrowth.

### **Oriented nanofiber meshes and directional outgrowth**

Schwann cells can secrete and maintain two different structures of laminin: a fibrillar construct typically indicative of young Schwann cells or low-passage cells *in vitro*, and a reticular construct more often seen with higher-passage cells or mature Schwann cells.<sup>31</sup> Because the fibrillar matrix state exists during development, it is highly probable this fibrillar laminin mesh provides important path-finding cues for the growth cones of developing neurons. By extension, this fibrillar structure may be particularly relevant in regeneration as it mimics the environment during development which may function to speed the regenerative capability of the peripheral nervous system. In our studies, we found attachment to be equivalent on aligned substrates and on random nanofiber substrates. In

particular, no differences were found with attachment on aligned fibers even when laminin was not included in the mesh. Since previous studies showed attachment to laminin-containing nanofibers as preferential over PCL only nanofibers, these data suggest that structural orientation as well as biochemical cues play critical roles in cell attachment.

### Rat tibial nerve transection recovery

With respect to functional recovery, we assessed motor and sensory function throughout the study, in addition to nerve conduction velocity, EMG, and tissue histology at the end of the study. In animals receiving empty conduits, little improvement is seen in either motor or sensory function, validating the 10 mm defect as a large gap that will not heal successfully within 6 weeks. Significant reduction in thermal withdrawal latency was observed with all conduits containing nanofibers, with laminin–PCL aligned nanofibers providing the best recovery through the first 4 weeks of the study. While this test is subject to some variability based on the environment, care was taken to maintain as many external variables constant as possible over the course of the study. The decreasing standard deviations over time, especially in the 6th week of the study, show that while individual animal response to the surgery may vary initially, healing responses have stabilized by the 6th week. By that time, most animals showed thermal withdrawal latency in the pre-operative range of 4–6 s. The decreasing trends in thermal withdrawal latency, as well as the companion decrease in withdrawal deviation suggests that a physical, nanoscale presence within the lumen of the conduit promotes faster outgrowth and functional recovery, regardless of the composition or orientation. Statistical differences in healing occur between weeks 4 and 6 across all groups, as latencies decrease to near un-operated response. While in this case thermal withdrawal latency was tested weekly, testing more often might elucidate a more exact point at which all animals return to their baseline levels. We expected to find laminin nanofibers within the conduit providing an ideal substrate for axonal attachment and extension; however, the latency data suggest alignment of nanofibers may be more critical than composition. Both PCL and laminin–PCL aligned nanofibers showed faster recovery to normal response than either composition of random nanofibers. In addition, laminin–PCL random nanofibers showed the slowest recovery of function. This surprising result may be due to the potential immunogenicity of laminin in this model. Initial healing may be slowed by the animals' immune reaction to the foreign protein; however, these animals still reach baseline latency levels by the end of 6 weeks.

Motor recovery was assessed by gait over time from pre-operative tracks as well as the un-operated control side. In this assessment, differences in motor recovery emerged based on the content and alignment of nanofibers within the conduit. Regardless of composition or orientation, nanofibers within the conduit provided for better recovery capabilities than a hollow conduit. When comparing the toe spread, animals receiving PCL nanofibers in the aligned configuration showed the most significant motor recovery when compared to hollow conduits, whereas randomly-oriented laminin nanofibers showed no significant difference in recovery over hollow conduits. In addition, conduits containing laminin blend aligned nanofibers approached significance when compared to hollow conduits and those containing randomly-oriented laminin blend nanofibers. These results suggest substrate alignment is critical for motor recovery. In this case, animals receiving randomly-oriented nanofibers

with laminin content showed minimal functional recovery over hollow conduits. Over the short duration of this study, it is possible that the animals' immune system was still mounting a response to the laminin content in the conduit, causing slightly greater inflammation in those surgery sites and affecting the animals' gait. However, when considering aligned conduits, perhaps the benefit of alignment outweighs any potential inflammatory effects of laminin, allowing animals with aligned laminin blend conduits to approach or in some cases surpass the functional recovery of animals that received aligned PCL nanofibers.

When examining the ability of regenerated nerves to conduct impulses, we measured conduction both anterograde and retrograde. Anterograde indicates forward conduction, or conduction continuing on toward the target organ. Retrograde indicates reverse conduction, or conduction away from the target organ. While trends were apparent in anterograde conduction, no significance was found; however, anterograde conduction is especially sensitive to outside interference. For example, if any extraneous tissue is not freed from the nerve, conduction is possible anterograde through the adhered muscle tissue. Fortunately, retrograde transmission is not as susceptible to this particular noise, and in this metric there are significant differences in nerve conduction velocity. As previously discussed, the presence of nanofibers within the lumen of the conduit does indeed promote faster outgrowth and greater functional recovery in terms of nerve conduction at the 6 week time point. Randomly oriented synthetic nanofibers provide a better surface than an empty conduit. However, regardless of composition, conduits containing aligned nanofibers demonstrated significantly greater reverse conduction velocities. The highest mean conduction velocity was achieved with laminin-PCL aligned nanofibers, perhaps because this construct most closely mimics both the structure (alignment) and composition (laminin content) of the native healing environment.

In future studies, we hope to develop a method for fixing the nanofiber meshes within the center of the conduit. Clements et al.<sup>9</sup> utilized custom machined templates to section their polysulfone guidance tubes; however, our PCL microfiber tubes would not stand up to this methodology. We are currently developing a method to section the nerve guidance conduits, insert the nanofiber mesh, and successfully re-seal the tube without losing the microfiber morphology or permeability, or generating a mechanically weak zone along the length of the conduit. In addition, methods to assess permeability of the microfiber guidance channels and the effects of varying permeability on nerve regeneration are being considered. Along with affecting cell infiltration, transport and diffusion through the conduit, changes in permeability may also affect cellular adhesion,<sup>32</sup> which could modify the exterior environment of the scaffold and influence scar tissue formation.

While blending of laminin and PCL here showed favorable functional outcomes after 6 weeks of regeneration, the possibility remains of immunogenicity due to the laminin content. To address this concern, future studies will focus on isolating the active sequence of the laminin molecule (e.g., IKVAV or YIGSR) and blending or performing surface modifications to determine if a single peptide is sufficient to recapitulate the bioactivity of laminin within the regenerating environment. Synthetic peptides would remove the potential for immune reaction to the mouse laminin used here; however, peptide sequences may not

substitute for the effects of the complete protein. If we find that to be the case, we will investigate the effectiveness of recombinant laminin molecules.<sup>33,34</sup>

## CONCLUSIONS

In conclusion, laminin-PCL blend nanofibers containing 10% by weight laminin maintain the bioactivity of pure laminin nanofibers in terms of cell adhesion and neurite extension. Alignment of nanofibers further increases the length of process extension. When used in the lumen of a conduit for peripheral nerve regeneration, the nanofiber structure provides significant benefit over a hollow conduit, with even greater benefit and faster healing seen with laminin content, and the fastest healing with alignment along the length of the conduit. These studies provide a firm foundation for the use of natural–synthetic blend electrospun nanofibers to enhance existing hollow nerve guidance conduits. The similarity in surgical technique and obvious benefit to the patient should lead to faster translation into clinical application.

## Acknowledgments

The authors would like to acknowledge the assistance of Vasudha Chaurey, from the laboratory of Dr. Nathan Swami in the Department of Electrical Engineering, with FFT analysis of fiber alignment, and Judy Warder from the EMG Lab at the University of Virginia Health System for her expertise and time in obtaining the electrophysiology measurements. The YFP-reporter transgenic mouse was a gift from Drs. Lui, Geisert, Frankfurter and Spano to Dr. Ogle. Benjamin Brooks, Heather Patel, and Alan Reyes assisted in blinded data collection from the animal study, Frank Block assisted in aligned nanofiber fabrication, and Tiffany Wang assisted in figure compilation.

Contract grant sponsor: National Science Foundation Emerging Frontiers in Research and Innovation (EFRI); contract grant number: 736002

Contract grant sponsor: National Institute of Dental & Craniofacial Research; contract grant number: DE-010369-08

Contract grant sponsor: University of Virginia Biotechnology Training Program; contract grant number: 5T32GM008715-08

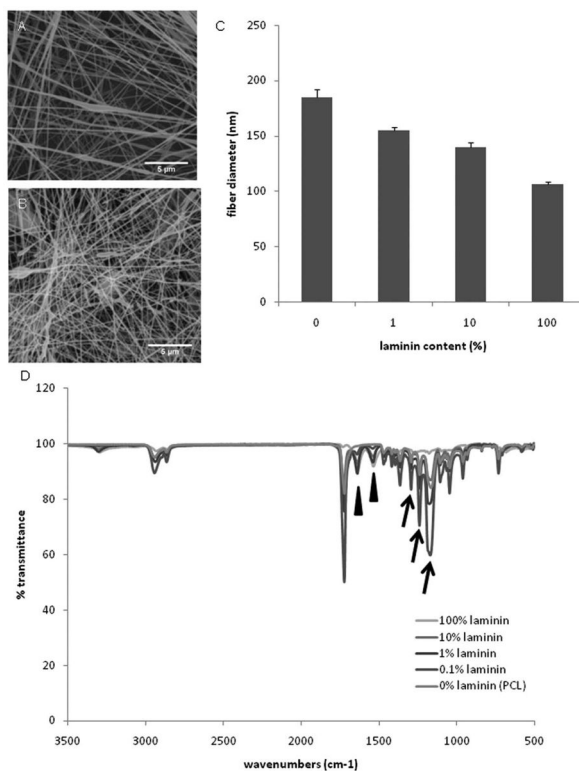
Contract grant sponsor: National Science Foundation Chemical, Bioengineering, Environmental, and Transport Systems (CBET); contract grant number: 0933643

## References

1. Burnett MG, Zager EL. Pathophysiology of peripheral nerve injury: A brief review. *Neurosurg Focus*. 2004; 16:E1. Review. [PubMed: 15174821]
2. Colen KL, Choi M, Chiu DT. Nerve grafts and conduits. *Plast Reconstr Surg*. 2009; 124(6 Suppl):e386–e394. [PubMed: 19952706]
3. Bellamkonda RV. Peripheral nerve regeneration: An opinion on channels, scaffolds and anisotropy. *Biomaterials*. 2006; 27:3515–3518. [PubMed: 16533522]
4. Hoke A. Mechanisms of disease: what factors limit the success of peripheral nerve regeneration in humans? *Nat Clin Pract Neurol*. 2006; 2:448–454. Review. [PubMed: 16932603]
5. Jiang X, Lim SH, Mao HQ, Chew SY. Current applications and future perspectives of artificial nerve conduits. *Exp Neurol*. 2010; 223:86–101. [PubMed: 19769967]
6. Schmidt CE, Leach JB. Neural tissue engineering: strategies for repair and regeneration. *Annu Rev Biomed Eng*. 2003; 5:293–347. Review. [PubMed: 14527315]
7. Kleinman HK, Philp D, Hoffman MP. Role of the extracellular matrix in morphogenesis. *Curr Opin Biotechnol*. 2003; 14:526–532. [PubMed: 14580584]

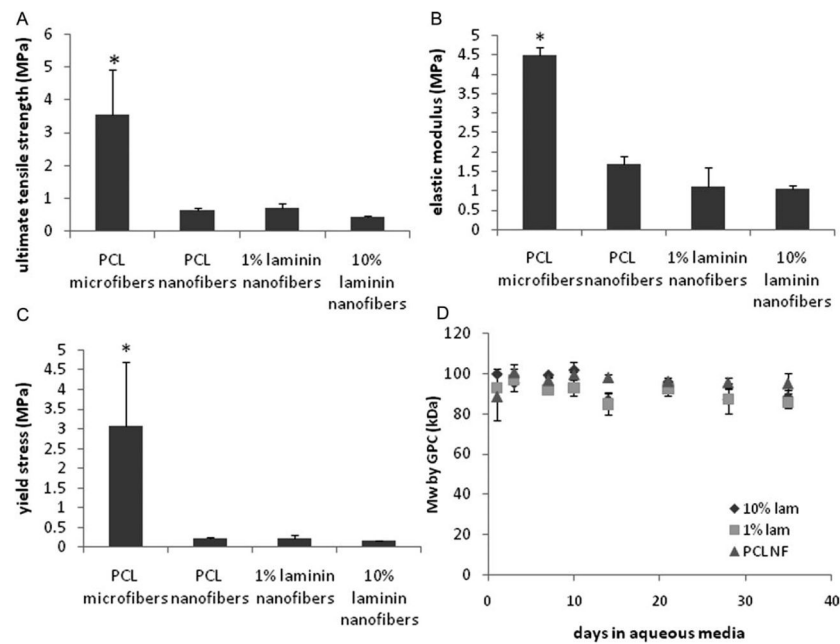
8. Neal RA, McClugage SG, Link MC, Sefcik LS, Ogle RC, Botchwey EA. Laminin nanofiber meshes that mimic morphological properties and bioactivity of basement membranes. *Tissue Eng Part C Methods*. 2009; 15:11–21. [PubMed: 18844601]
9. Clements IP, Kim YT, English AW, Lu X, Chung A, Bellamkonda RV. Thin-film enhanced nerve guidance channels for peripheral nerve repair. *Biomaterials*. 2009; 30:3834–3846. [PubMed: 19446873]
10. Kim YT, Haftel VK, Kumar S, Bellamkonda RV. The role of aligned polymer fiber-based constructs in the bridging of long peripheral nerve gaps. *Biomaterials*. 2008; 29:3117–3127. [PubMed: 18448163]
11. Chaurey V, Chiang P, Polanco C, Su Y, Chou C, Swami N. Interplay of electrical forces for alignment of sub-100 nm electrospun nanofibers at insulator gap collectors. *Langmuir*. 2010; 26:19022–19026. [PubMed: 21082824]
12. Abrams GA, Schaus SS, Goodman SL, Nealey PF, Murphy CJ. Nanoscale topography of the corneal epithelial basement membrane and Descemet's membrane of the human. *Cornea*. 2000; 19:57–64. [PubMed: 10632010]
13. Kakade MV, Givens S, Gardner K, Lee KH, Chase DB, Rabolt JF. Electric field induced orientation of polymer chains in macroscopically aligned electrospun polymer nanofibers. *J Am Chem Soc*. 2007; 129:2777–2782. [PubMed: 17302411]
14. Hannan GN, Reilly W. Adsorption from fetal calf serum of collagen-like proteins which bind fibronectin and promote cell attachment. *Exp Cell Res*. 1988; 178:343–357. [PubMed: 2458951]
15. Bethea CL, Borg TK. PC12 cell aggregation and dopamine production on EHS-derived extracellular matrix. *Mol Cell Endocrinol*. 1988; 58:113–128. [PubMed: 3061856]
16. Liu L, Geisert EE, Frankfurter A, Spano AJ, Jiang CX, Yue J, Dragatsis I, Goldowitz D. A transgenic mouse class-III  $\beta$  tubulin reporter using yellow fluorescent protein. *Genesis*. 2007; 45:560–569. [PubMed: 17868115]
17. Jiang M, Zhuge X, Yang Y, Gu X, Ding F. The promotion of peripheral nerve regeneration by chitooligosaccharides in the rat nerve crush injury model. *Neurosci Lett*. 2009; 454:239–243. [PubMed: 19429091]
18. Bain JR, Mackinnon SE, Hunter DA. Functional evaluation of complete sciatic, peroneal and posterior tibial nerve lesions in the rat. *Plast Reconstruct Surg*. 1989; 83:129–136.
19. Li D, Wang YL, Xia YN. Electrospinning of polymeric and ceramic nanofibers as uniaxially aligned arrays. *Nano Lett*. 2003; 8:1167–1171.
20. Wei SY, Zhang PX, Han N, Dang Y, Zhang HB, Zhang DY, Fu ZG, Jiang BG. Effects of Hedysari polysaccharides on regeneration and function recovery following peripheral nerve injury in rats. *Am J Chin Med*. 2009; 37:57–67. [PubMed: 19222112]
21. Mecerreyes D, Stevens R, Nguyen C, Pomposo JA, Bengoetxea M, Grandea H. Synthesis and characterization of polypyrrole-*graft*-poly(epsilon-caprolactone) copolymers: New electrically conductive nanocomposites. *Synth Met*. 2002; 126:173–178.
22. Polo Fonseca C, Cavalcante F Jr, Amaral FA, Zani Souza CA, Neves S. Thermal and conduction properties of a PCL-biodegradable gel polymer electrolyte with LiClO<sub>4</sub>, LiF<sub>3</sub>CSO<sub>3</sub>, and LiBF<sub>4</sub> Salts. *Int J Electrochem Sci*. 2007; 2:52–63.
23. Elzein T, Nasser-Eddine M, Delaite C, Bistac S, Dumas P. FTIR study of polycaprolactone chain organization at interfaces. *J Colloid Interface Sci*. 2004; 273:381–387. [PubMed: 15082371]
24. Huang YC, Huang CC, Huang YY, Chen KS. Surface modification and characterization of chitosan or PLGA membrane with laminin by chemical and oxygen plasma treatment for neural regeneration. *J Biomed Mater Res A*. 2007; 82:842–851. [PubMed: 17335016]
25. Li M, Mondrinos MJ, Chen X, Lelkes PI. Electrospun blends of natural and synthetic polymers as scaffolds for tissue engineering. *Conf Proc IEEE Eng Med Biol Soc*. 2005; 6:5858–5861. [PubMed: 17281592]
26. Lee KH, Kim HY, Khil MS, Lee DR. Characterization of nano-structured poly(epsilon-caprolactone) nonwoven mats via electrospinning. *Polymer*. 2003; 44:1287–1294.
27. Pektok E, Nottelet B, Tille JC, Gurny R, Kalangos A, Moeller M, Walpoth BH. Degradation and healing characteristics of small-diameter poly(epsilon-caprolactone) vascular grafts in the rat systemic arterial circulation. *Circulation*. 2008; 118:2563–2570. [PubMed: 19029464]

28. Pierucci A, Duek EA, de Oliveira AL. Expression of basal lamina components by Schwann cells cultured on poly(lactic acid) (PLLA) and poly(caprolactone) (PCL) membranes. *J Mater Sci Mater Med.* 2009; 20:489–495. [PubMed: 18987957]
29. Ketschek AR, Jones SL, Gallo G. Axon extension in the fast and slow lanes: Substratum-dependent engagement of myosin II functions. *Dev Neurobiol.* 2007; 67:1305–1320. [PubMed: 17638383]
30. Varnum-Finney B, Reichardt LF. Vinculin-deficient PC12 cell lines extend unstable lamellipodia and filopodia and have a reduced rate of neurite outgrowth. *J Cell Biol.* 1994; 127:1071–1084. [PubMed: 7962069]
31. Tsiper MV, Yurchenco PD. Laminin assembles into separate basement membrane and fibrillar matrices in Schwann cells. *J Cell Sci.* 2002; 115 (Part 5):1005–1015. [PubMed: 11870219]
32. Kwon IK, Kidoaki S, Matsuda T. Electrospun nano- to microfiber fabrics made of biodegradable copolyesters: Structural characteristics, mechanical properties and cell adhesion potential. *Biomaterials.* 2005; 26:3929–3939. [PubMed: 15626440]
33. Rodin S, Domogatskaya A, Ström S, Hansson EM, Chien KR, Inzunza J, Hovatta O, Tryggvason K. Long-term self-renewal of human pluripotent stem cells on human recombinant laminin-511. *Nat Biotechnol.* 2010; 28:611–615. [PubMed: 20512123]
34. Sasaki T, Takagi J, Giudici C, Yamada Y, Arikawa-Hirasawa E, Deutzmann R, Timpl R, Sonnenberg A, Bächinger HP, Tonge D. Laminin-121—Recombinant expression and interactions with integrins. *Matrix Biol.* 2010; 29:484–493. [PubMed: 20566382]



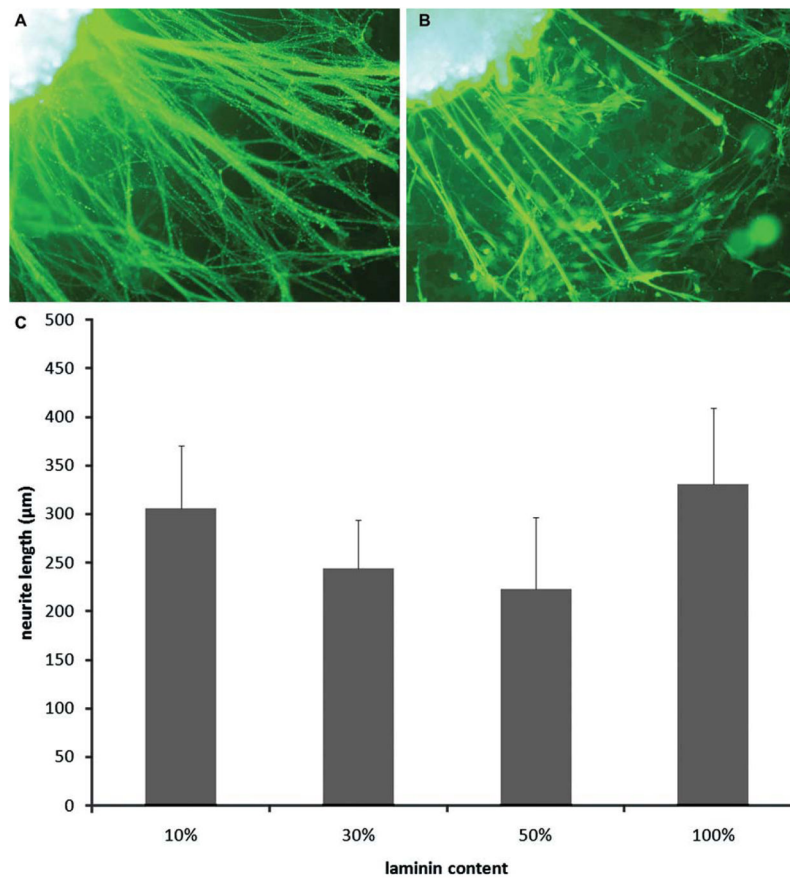
**FIGURE 1.**

Electrospun nanofibers of blended laminin and PCL. Representative scanning electron micrographs of electrospun laminin-PCL blend nanofibers containing (A) 1% and (B) 10% laminin in total polymer weight. All other parameters were kept constant. When mean fiber diameters were compared with respect to laminin content (C), no significant differences were found ( $p > 0.05$ ). Error bars depict standard error. (D) Fourier-transform infrared spectra indicate the presence of both PCL (arrows) and laminin (arrowheads) peaks in laminin-PCL blend nanofibers. Laminin peaks represent amine ( $1649\text{ cm}^{-1}$ ) and amide bond ( $1564\text{ cm}^{-1}$ ,  $1649\text{ cm}^{-1}$ ) regions, and PCL peaks represent C–O and C–C stretching ( $1293\text{ cm}^{-1}$ ), asymmetric COC stretching ( $1240\text{ cm}^{-1}$ ) and symmetric COC stretching ( $1170\text{ cm}^{-1}$ ).

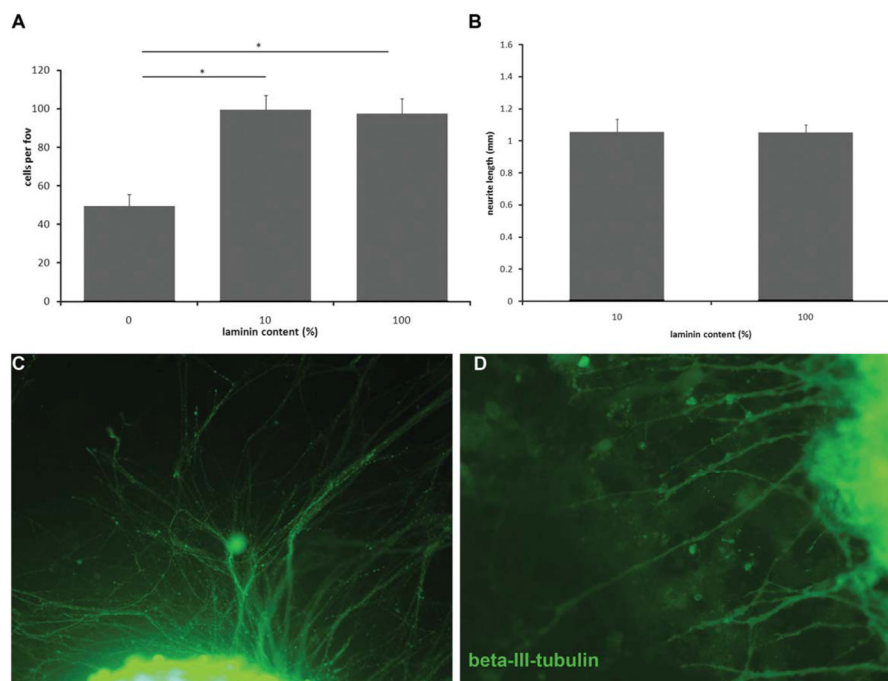
**FIGURE 2.**

Tensile and degradation properties of laminin-PCL blend nanofibers. (A) Young's moduli, (B) yield stress, and (C) UTS were calculated from stress-strain curves generated by uniaxial tensile testing. Young's moduli were estimated in the linear portion of the curve, between 5 and 25% strain, with UTS was reported as the maximal stress on the curve.

\*Indicates statistically significant difference ( $p < 0.05$ ) between microfiber group and all other groups. (D)  $M_w$  as measured by GPC did not change significantly over the lifetime of the conduit, regardless of the laminin content used. While a slightly decreasing trend is visible in the data, the change was not significant over time ( $p = 0.325$ ). Data were analyzed using a general linear model ANOVA with crossed factors in Minitab statistical software. Significance was asserted at  $p < 0.05$ . All error bars depict standard error.

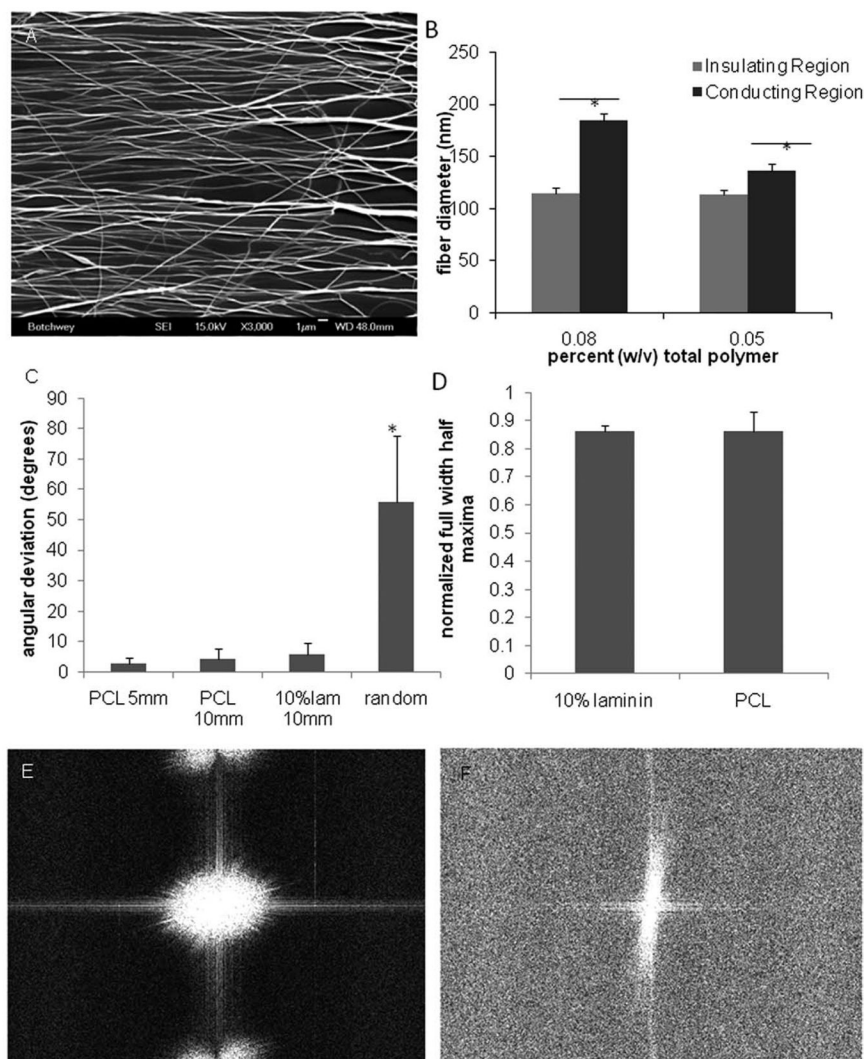


**FIGURE 3.** Process extension of isolated DRG on laminin and laminin-PCL blend films. Representative images of murine dorsal root ganglia (DRG) extending processes on (A) 100% and (B) 10% laminin films. (C) Process extension length on 10% laminin films is not significantly different from length on 30%, 50%, or even 100% laminin films. [Color figure can be viewed in the online issue, which is available at [wileyonlinelibrary.com](http://wileyonlinelibrary.com).]

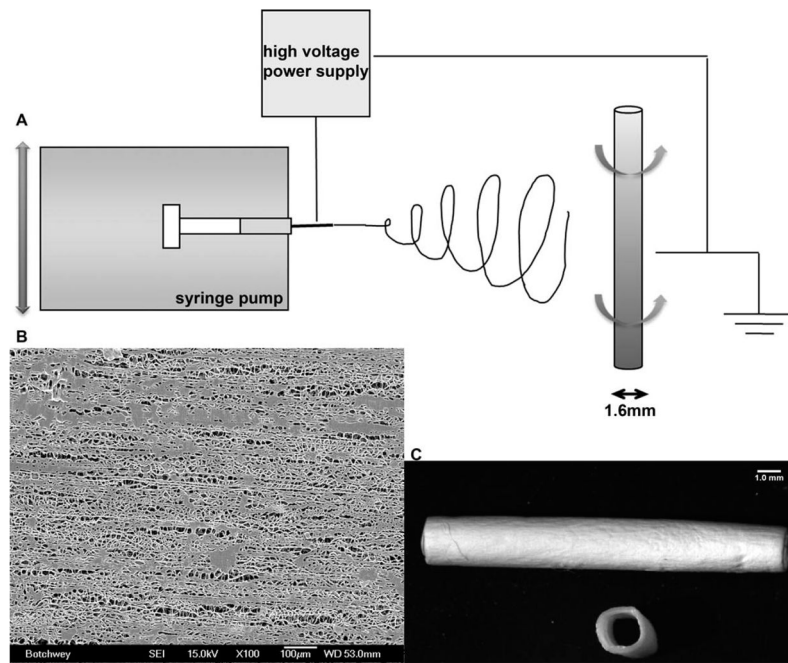


**FIGURE 4.**

Attachment and process extension on laminin and laminin-blend nanofibers. (A) PC12 cell attachment in serum free media on laminin-PCL blend nanofibers. \*Indicates  $p < 0.01$ . (B) Neurite extension length from DRG is not statistically different on laminin or laminin-PCL blend nanofibers, as illustrated by representative images of murine DRG neurite outgrowth on (C) 100% and (D) 10% laminin nanofibers after 4 days in NGF-supplemented culture conditions. All error bars represent standard error. [Color figure can be viewed in the online issue, which is available at [wileyonlinelibrary.com](http://wileyonlinelibrary.com).]

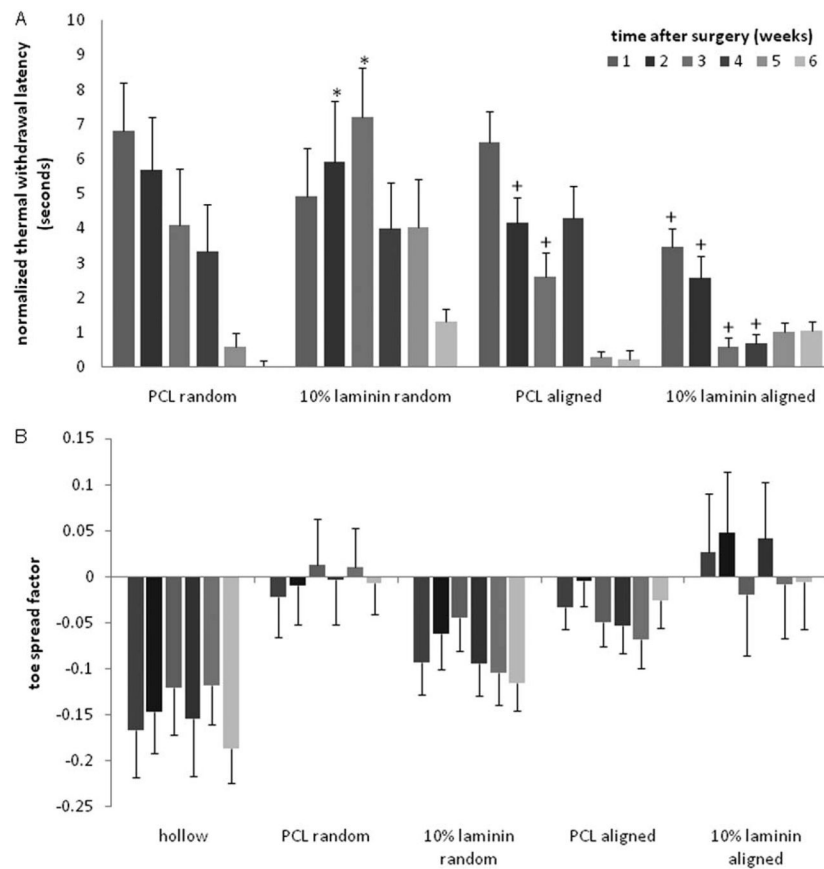


**FIGURE 5.** Stretching and alignment of laminin-PCL blend nanofibers using insulating gap. (A) Representative scanning electron micrograph of aligned 10% laminin blend nanofibers. (B) These nanofibers show significant stretching across the gap, resulting in decreased fiber diameter in aligned samples, regardless of initial total polymer weight (5% or 8%). (C) Degree of alignment was calculated using angular deviation from the axis of alignment, and no significant differences were found among aligned samples of PCL or laminin-PCL blend. (D) FFT calculations of normalized full width of half maximum frequency showed no statistically significant difference in degree of alignment between PCL and laminin-PCL blend nanofibers. Representative images of (E) randomly oriented and (F) aligned PCL nanofibers illustrate the effectiveness of insulating gap alignment.

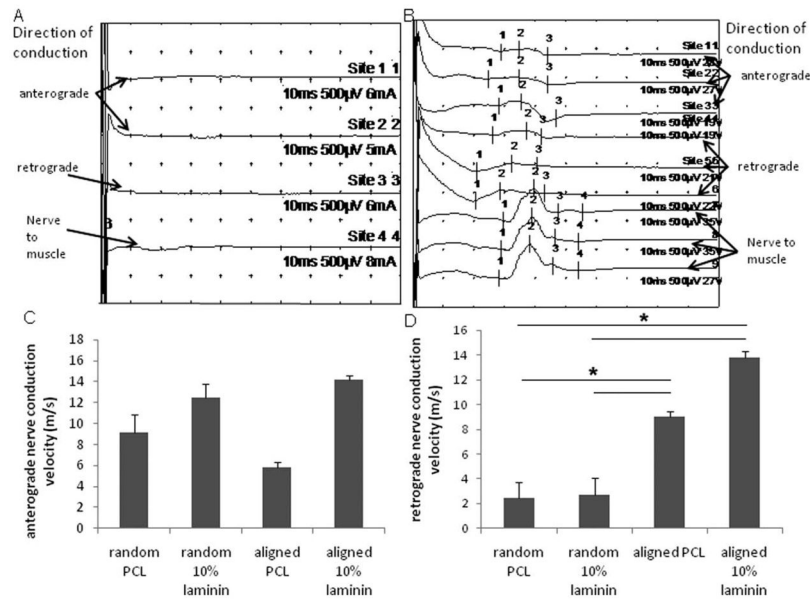


**FIGURE 6.**

Conduit fabrication. (A) Conduits were fabricated of PCL microfibers by electrospinning onto a rotating and translating mandrel. The diameter of the mandrel (1.6 mm) forms the inner diameter of the conduits. Mandrel rotation speed was set to 100 rpm to prevent mechanical alignment that occurs with higher rotation speeds. (B) Microfiber structure was confirmed by scanning electron microscopy. (C) Conduits were cut into 15 mm segments, nanofibers were inserted, and the conduits were sterilized for implantation.

**FIGURE 7.**

Effects of composition and orientation on sensory and motor response. (A) All conduits containing nanofibers showed decreasing thermal withdrawal latency periods over time. Data indicate operated leg response time normalized to un-operated leg response time. No significant differences were found among un-operated legs or sham operated legs. \*Indicates significant difference from sham ( $p < 0.05$ ), + indicates significant difference from hollow. (B) Motor response was measured by changes in toe spread factor. Toe spread typically decreases with tibial nerve deficits, as evidenced by the hollow conduits. PCL random and aligned perform better than 10% laminin random; however, 10% laminin aligned shows less shift than PCL aligned, and may therefore indicate fastest return to normal toe spread. Error bars represent standard error.

**FIGURE 8.**

Electrophysiology: Nerve conduction velocity. Sample electrode traces show electrophysiological response in (A) empty conduits and (B) conduits containing nanofibers after 6 weeks. Direction of stimulation is indicated on the plots. No impulses were recorded in animals with empty conduits. Electrode placement for anterograde conduction was stimulating electrode proximal to injury site, recording electrode distal; placement for retrograde conduction was stimulating electrode distal to injury site, recording electrode proximal; placement for nerve to muscle conduction was stimulating electrode proximal to injury site, recording electrode in the belly of the gastrocnemius muscle. Nerve conduction velocity was calculated from latencies (ms) using the distance between electrodes (mm). (C) Anterograde conduction velocity indicates stimulation proximal to injury and recording distal to injury site. (D) Retrograde conduction velocity indicates stimulation distal to injury and recording proximal to injury site. Forward conduction velocity appears greater with laminin content, but data were not significant ( $p > 0.05$ ). Retrograde conduction velocity was significantly greater when animals received conduits containing aligned nanofibers ( $p < 0.01$ ). All conduits containing nanofibers showed significantly greater conduction velocity in both directions than empty conduits ( $p < 0.001$ ).

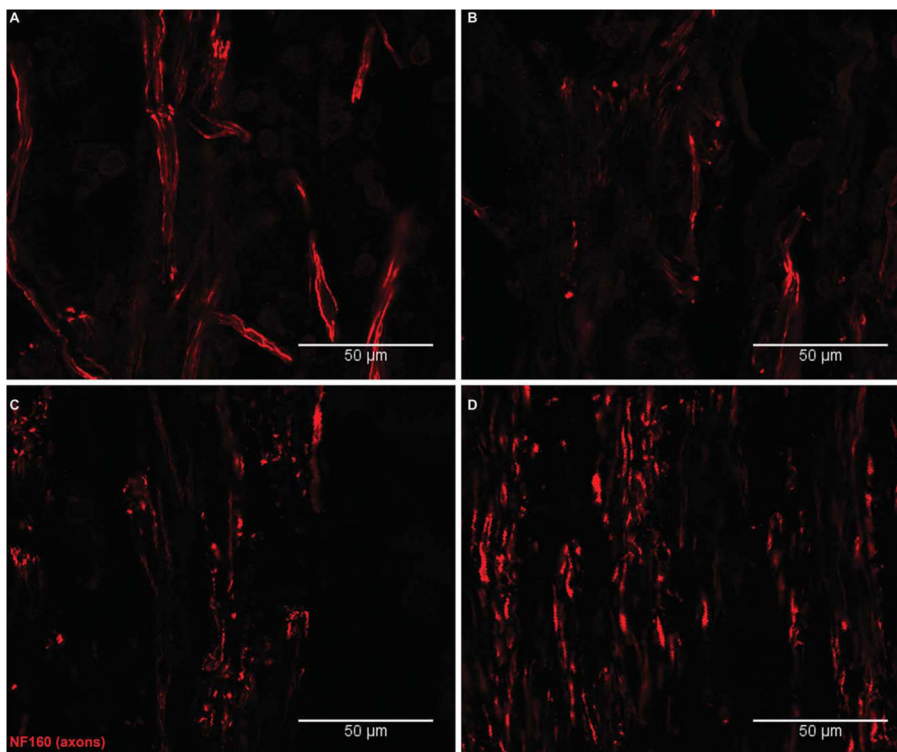


**FIGURE 9.**

Axonal regeneration within the conduit. Representative confocal micrographs showing immunohistochemistry for NF160, an axonal marker. A: PCL random and (B) laminin blend random have some tissue in-growth from proximal end to midline, but the neurons tend to be more spread out and less organized than when the nanofibers are aligned. Both (C) PCL aligned and (D) laminin-PCL blend aligned show greater density of axonal staining, suggesting greater tissue regrowth. The aligned images also show greater alignment of the re-growing neurons. All images are oriented with the proximal stump toward the bottom, with re-growth occurring upward. [Color figure can be viewed in the online issue, which is available at [wileyonlinelibrary.com](http://wileyonlinelibrary.com).]

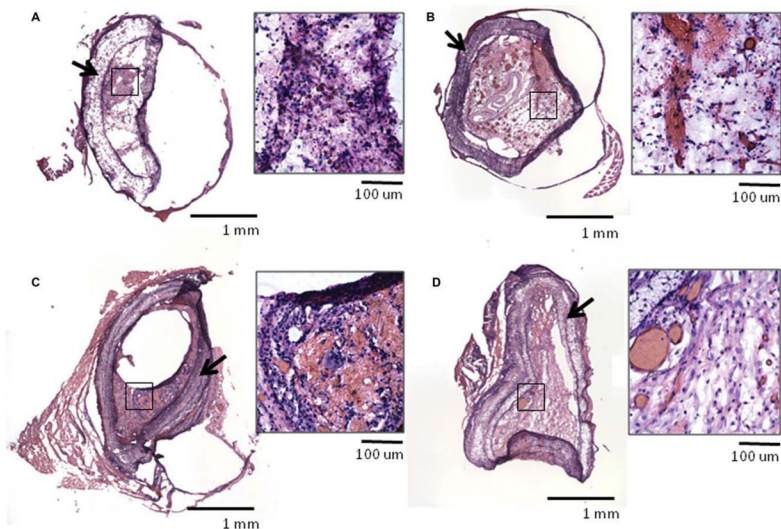


**FIGURE 10.**

Tissue in-growth into conduit. H&E stained cross-sections of nerve conduit implants taken from the center of the conduit. Conduits contained (A) PCL random, (B), laminin blend random, (C) PCL aligned, or (D) laminin blend aligned nanofibers within the lumen of the conduit. Insets show 40× magnification of black box on cross-section image to provide detailed tissue structure. The presence of laminin (B,D) resulted in increased cellular infiltration into the conduits. Fiber alignment compared to random fibers further improved tissue re-growth. [Color figure can be viewed in the online issue, which is available at [wileyonlinelibrary.com](http://wileyonlinelibrary.com).]